Proceedings of the 21st National & 10th ISHMT-ASME Heat and Mass Transfer Conference
ISHMT2011
December 27-30, 2011, IIT Madras, India

ISHMT_USA_018

DESIGN OF A MICROCHANNEL BASED SOLAR RECEIVER/REACTOR FOR BIOFUEL PROCESSING

Kevin Drost
School of Mechanical, Industrial and Manufacturing Engineering
Oregon State University
Corvallis, Oregon 97331
Email: drostk@onid.oregonstate.edu

Sourabh V. Apte
School of Mechanical, Industrial and Manufacturing Engineering
Oregon State University
Corvallis, Oregon 97331
Email: sva@engr.orst.edu

John Schmitt
School of Mechanical, Industrial and Manufacturing Engineering
Oregon State University
Corvallis, Oregon 97331
Email: schmitjo@engr.orst.edu

Vinod Narayanan
School of Mechanical, Industrial and Manufacturing Engineering
Oregon State University
Corvallis, Oregon 97331
Email: vinod.narayanan@oregonstate.edu

ABSTRACT

This study investigates use of solar thermochemical processing of clean fuels using biomass products (CH_4, CO_2, H_2O*). To address technological feasibility of a microchannel-based solar receiver/reactor a combined numerical and experimental study of methane-steam reforming is carried out on a single microchannel with Palladium-deposited channel walls and heat input to facilitate endothermic heterogeneous reactions producing hydrogen. A simple one-dimensional model solving steady state species mass fraction, energy, and overall conservation of mass equations is developed and verified against the full, three-dimensional direct numerical simulation studies as well as experimental data by Eilers and co-workers [1, 2]. Methane-steam reforming is modeled by three reduced-order reactions occurring on the reactor walls. The effects of the total heat input, heat flux profile, and inlet flow rate on production of hydrogen are investigated in detail to assess the effectiveness of the microchannel configuration for production of hydrogen. A shape-optimization procedure is developed and applied to design the solar receiver shape that can yield a desired heat flux distribution along the microchannel walls. This constrained nonlinear optimization problem was solved in Matlab using SNOPT. A coupled optimization and Monte-Carlo radiative heat transfer model is developed to design the receiver shape.*

INTRODUCTION

Solar energy is a promising clean energy source that is of great economic and technological importance. Typically, one of two conversion pathways are followed in converting solar energy to usable energy: (a) direct electrical power through photovoltaics, and (b) chemical processing and production of hydrogen or other fuels [3–6]. The present work is motivated from the perspective of trying to address important technological challenges that could enable efficient solar thermochemical processing of clean fuels using biomass products (CO_2, CH_4).

Technological issues for solar thermochemical processing can be classified into: (a) design of solar concentrators that permit energy collection at high efficiency, (b) receiver designs that will increase the chemical efficiency of an endothermic reaction for biofuel reforming, and (c) process control schemes that could

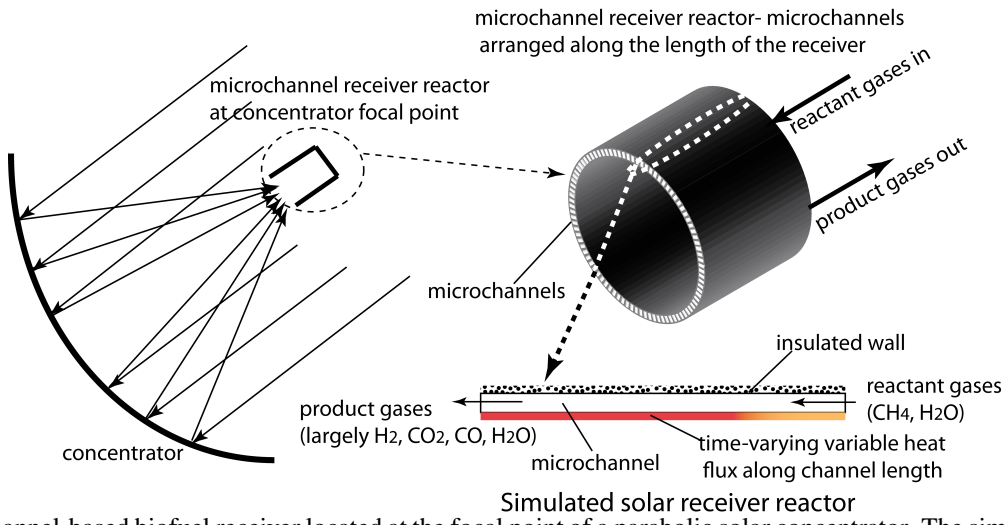

FIGURE 1: Microchannel-based biofuel receiver located at the focal point of a parabolic solar concentrator. The simulated reactor is used in the present study. The receiver shape, comprised of multiple microchannel reactors,is obtained from shape-constrained optimization.

optimize the production of fuels. The technological readiness of solar concentrators is relatively high [6, 7]; however, significant improvements can be made to the receiver designs and process control to permit increased efficiencies of the receiver and chemical reforming. Solar receivers based on a volumetric or cavity receiver design are common [8–10], wherein chemical reactions occur in cylindrical cavities by constraining the reactants and products within the cavity. Chemical reactions in such chambers could be limited by (i) the diffusion time of the non-premixed reactants, (ii) low heat transfer rates from the walls to the reactants, and (ii) low volumetric absorption by the reactant gases.

The present work investigates conversion efficiency of biomass-based gaseous products (CH_4,CO_2) using a microchannel-based reactor, as shown in Figure 1. This design exploits the short diffusion lengths for reactant gases in microchannels, such that the reaction may occur near stoichiometric conditions (using very less excess reactant gases), thereby substantially increasing the efficiency of the system. In order to study the technical feasibility of such a design, we first investigate, through numerical simulations, the strong endothermic reactions of methane-steam reforming inside a microchannel reactor with *Palladium* catalyst. The simulations are based on the experimental setup by Eilers [1]. Previous work [11] also involved detailed numerical simulation using a low-Mach number, unsteady, variable-density Navier-Stokes equations together with species mass-fraction and energy equations solved for a three-dimensional microchannel configuration.

The primary goal of the present work is to develop a simple one-dimensional model for the thermochemical processes inside the reactor. The main reason to develop such model is to facilitate several parametric studies that can be used to obtain operation range as well as conditions for improved hydrogen production. The goal is to investigate the effect of inlet flow rate, the net heat input, and distribution of input heat flux profile on the species diffusion, physicochemical reactions and heat transfer processes inside the microchannel reactor.

The second objective of this work is to develop methodology that will provide shape of the receiver necessary to obtain a desired heat flux distribution along the microchannel walls. Specifically, knowing the heat flux distribution and other conditions that produce improved hydrogen production, the goal is to design the receiver shape that will yield such a distribution. This requires solution of the radiative heat transfer problem (done using the MONT2D software [12]) that provides shape factors for a chosen receiver geometry. Next, the radiative solver is coupled with a shape-constrained optimization procedure to obtain a receiver shape that will closely provide the desired heat flux distribution through an iterative approach.

SETUP and MATHEMATICAL FORMULATION

The experimental setup for the present study corresponds to the single microchannel considered by Eilers [1] The heat input through bottom wall of the microchannel is provided by blow torches impinging directly on the wall, simulating solar energy flux. The catalyst used here was a porous felt with deposited palladium nanoparticles throughout the felt (chemical kinetics characteristic are taken from Shu *et al.* [13]). For the case studied in this work (catalyst C), the channel wall was treated such that Palladium nanoparticles were deposited uniformly throughout the surface to give a porous catalyst bed (see Eilers *et al.* [2] for details) The height of the channel is 0.86 *mm* with a total length of 0.1735 *m* and a catalyst length of 0.133 *m*, the width of the channel is 19 *mm* in the catalyst section (the section of the channel). A three-dimensional model was used in the previous DNS studies [11]. In the present one-dimensional model, the inlet and outlet pipe sections are not considered and model equations are

solved only along the microchannel.

To perform parametric studies varying inlet steam-to-methane ratio, inlet temperature, surface heat distribution, and net surface heat flux, a simplified one-dimensional reacting flow model for *steady state* solution was developed. Using a simple staggered grid and neglecting diffusion in the wall-normal direction, the following steady state equations can be derived:

$$\frac{d}{dx}(\rho\bar{u}) = \frac{d}{dx}(\dot{m}'') = 0 \tag{1}$$

$$\frac{d}{dx}(\dot{m}''Y_i) = \frac{d}{dx}\left(\rho D\frac{dY_i}{dx}\right) + \dot{\omega}_i''' \tag{2}$$

$$\frac{d}{dx}(\dot{m}''h_s) = -\frac{d\dot{q}''}{dx} - \sum_i^{N_s}\dot{\omega}_i'''h_{f_i}^o. \tag{3}$$

where $\bar{u}$ is the average velocity over the cross-section of the microchannel, N_s, ρ, Y_i, p, $h_s = \int_{T_{ref}}^{T} c_{p_{mix}}dT$, and $\dot{q}''$, represent the number of species transport equations, density, species mass fraction, mixture specific enthalpy, and heat flux due to conduction and species diffusion, respectively. The mixture is assumed as an ideal gas with the viscosity, thermal conductivity, and the binary diffusion coefficient ($\mathscr{D}_{i,m}$) depending upon the local composition and temperature. Also $\dot{\omega}_i'''$ represents source terms corresponding to the homogeneous gas-phase reactions in the species mass fraction. Corresponding source in the energy equation is based on the species heat of formation, $h_{f_i}^o$. The mixture density is obtained from the ideal gas equation.

The majority of chemical conversion takes place on the catalyst surface giving rise to heterogeneous reactions modeled by the three surface reactions 4, 5, 6. Using a finite volume approach and integrating the one-dimensional model over the control volume, implementation of the surface reactions and surface heat flux into this model is fairly straight forward. The coupled equations for mass, species concentrations, and energy are solved using an iterative successive over-relaxation scheme. The species advection terms are discretized using a second-order Beam-Warming scheme, properties at the fluxes are evaluated using simple arithmetic averages, and diffusive fluxes are approximated using a piecewise linear profile assumption (resulting in a symmetric central differencing). Solution is obtained within only a few seconds on a laptop.

Chemical Kinetics for Heterogeneous Reactions

In the microchannel-based solar reactor, chemical reactions can occur in the gaseous phase as well as a series of reactions on the catalyst surface. Past studies by Deutschmann & Schmidt [14] on oxidation of steam in a tubular model showed that for atmospheric pressures, the gas-phase reactions contributed negligibly to the oxidation process In the present work, experiments are conducted at atmospheric conditions and the gas-phase reactions are neglected. The surface chemical reactions are modeled as boundary conditions to the energy and species equations for a reduced reaction mechanism of methane-steam reforming [15, 16, 16–18]:

$$CH_4 + H_2O \Longleftrightarrow CO + 3H_2; \quad \Delta H_{298}^0 = +206 \text{ kJ/mol} \tag{4}$$

$$CO + H_2O \Longleftrightarrow CO_2 + H_2; \quad \Delta H_{298}^0 = -41 \text{ kJ/mol} \tag{5}$$

$$CH_4 + 2H_2O \Longleftrightarrow CO_2 + 4H_2; \quad \Delta H_{298}^0 = +165 \text{ kJ/mol}. \tag{6}$$

The catalytic reaction rates are nonlinear relations comprising the reactant species concentrations and the local temperature. A reduced reaction mechanism with the following two endothermic (equations 4,6) and one exothermic water-gas shift (equation 5) global reactions was used to model the chemical conversion. To calculate the reaction rates, the classical kinetic model was employed [20, 21]. As mentioned earlier, the catalyst used here was a porous felt with deposited palladium nanoparticles throughout the felt (chemical kinetics characteristics are taken from Shu *et al.* [13]). In order to account for this distribution in the numerical model, it is necessary to quantify the surface distribution of the deposited Palladium catalyst. However, since the bed is porous, it is not straightforward to model its effect on the reaction rates. In the present work, a *reaction-rate correction factor*, α_s, that modifies the pre-exponential factor in the Arrhenius reaction rates (equation 7) is introduced. Experimental data is used to obtain this reacton-rate correction factor as explained in the results section. Thus, the reaction reaction rates for each chemical reactions can be formulated as

$$r_k = k_{f,k}\Pi_{i=1}^{N_s}[\mathrm{C}_i]^{\nu'_{ki}}, \tag{7}$$

$$k_{f,k} = \alpha_s A_k \exp\left(-\frac{E_{a,k}}{RT}\right). \tag{8}$$

where C_i denotes the concentration per unit volume of the i^{th} chemical species in the mixture, $k_{f,k}$ is the specific reaction rate constant for the k^{th} reaction and ν'_{ki}, which is dimensionless, is the stoichiometric coefficient of the i^{th} chemical species in the k^{th} reaction. The reaction activation energy ($E_{a,k}$), the activation constants A_k and α_k for each k^{th} reaction is obtained from the experimental data [17, 18] for a specific catalyst and are given in Drost *et al.* [11]. With the above surface reaction rates, the catalytic conversion is then modeled simply through boundary conditions for the species mass-fractions and temperature equations [14, 15] as described in detail by Drost *et al.* [11].

NUMERICAL RESULTS

The numerical approach together with the Arrhenius-type surface reaction rate model [11] were validated against the numerical studies on micrchannel methane-steam reforming performed by Kuznetsov and Koslov [15] using a Nickel catalyst. Their work uses the commonly used reaction rate model based on packed-bed reactor experiments by Hou and Hughes [18]. Accurate reproduction of these results (not shown here, published

in Drost *et al.* [11]) were necessary to verify proper implementation of the chemical kinetics models in the full DNS solver. The steady-state 1D model was first used to obtain the reaction rate correction factor by performing calibration studies based on matching the exit hydrogen concentrations with experimental data [1, 2]. The model results were also compared with past DNS studies to show good predictive capability.

For specified inlet flowrates, steam-to-methane ratio and net heat flux into the reactor, the α_s value was varied to match the bulk exit molar concentration for H_2 with the experiments. The heat fluxes going into each section were not available, rather the total heat input into the reactor was obtained from experiments by doing an overall energy balance. The heat input was assumed uniformly distributed along the microchannel surface. The α_s values for each case varied slightly. The mean reaction rate correction factor was obtained to be 6.6×10^{-5}, indicating that the active catalyst sites were a small fraction, consistent with the visual observations in the SEM images [2]. Once this averaged reaction-rate correction factor was determined, it was kept constant and all the cases were run again to establish the errors in numerically predicted exit hydrogen concentrations compared to experimental measurements. Errors less than 16% were observed for all cases and are within the experimental uncertainty given considerable heat losses observed in the experimental facility [2].

Parametric Studies Investigating H_2 Production

The validated 1D model was used to perform parametric studies varying the net heat input to the reactor, the heat flux profile (constant, ramp up, ramp down) along the channel, and the inlet flow rates. Only representative results are shown here owing to space constraints.

Net Heat Input The effect of external heat flux on H_2 production is investigated as the reaction rates are highly dependent on the local surface temperature. Three heat flux magnitudes were enforced at mean values of 2, 3 and 4 kW/m^2 with uniform distribution along the channel wall. The corresponding amount of heat input was 394.5, 450.9 and 511.05 W, respectively. The steam-methane ratio was set to 2.7 (case C7) and the flow rate at $0.183 g/min$. With increase in the amount of heat flux, the H_2 production as well as reaction rates at the wall increased, as expected. Increased value of heat flux increases the temperature along the wall, leading to enhanced H_2 production. The average temperatures for these cases over the reactor were 1145.7, 1170.3 and 1194.3 K, respectively.

The reaction rates (for R3) plot (not shown) showed maximum reaction near the entrance with continuous decrease in the reaction rate along the channel. The overall reaction rate values were higher for the higher heat flux input. The premixed H_2O-CH_4 mixture diffuses to the catalyst surface and reacts to produce hydrogen. Production of H_2 is an endothermic reaction, and this causes the temperature at the wall to initially decrease. Reactions continue to occur along the channel wall, however, their rate is decreased. For all cases, the reaction rates went down after the mid-section, and the temperature increased owing to thermal heating of the gases. For the cases studied, only 26.9% of the initial methane was converted to hydrogen, which is similar to the experimental observation. This may be attributed to small residence times compared to the reaction time scales as well as non-uniformity of reaction sites on the porous surface.

Heat Flux Profile Since methane-steam reforming is an endothermic reaction, the temperature values near the catalyst wall are bound to drop in the absence of heat addition. However, in order to explore the effect of heat-flux profile on the non-linear nature of the reaction rates and H_2 production, three different heat flux profiles were considered: uniform distribution, ramp up, and ramp down wherein the heat flux is varied linearly along the channel walls. For all cases, the average heat flux over the microchannel length was kept fixed (three different values were studied as before) and the steam-methane ratio was set to 2.7 (case C7) and the flow rate at $0.183 g/min$.

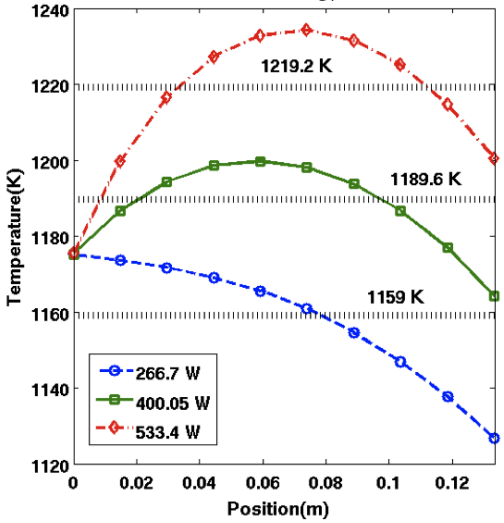

FIGURE 2: Temperature distribution along the reactor for different decreasing heat flux distributions. Also shown are the corresponding average reactor temperatures.

The most interesting case is that of the decreasing heat flux profile. Figure 2 shows the variation of catalyst temperature along the reactor for three different net heat inputs. It is observed that the mean reactor temperatures were larger for this case compared to the uniform and decreasing ramp heat flux distributions. For the highest heat input of 533.4 W, the temperature of the reactor actually increases in the first half of the channel and then decreases. Since endothermic reactions are occurring in the first half, having larger heat flux (decreasing ramp), seems to benefit the reaction rates and net exit hydrogen production. This suggests that using decreasing ramp for heat flux distribution is important and makes use of the input heat for actual methane

conversion rather than thermal heating of the product gases as observed in the uniform and increasing heat flux profiles. The hydrogen production (based on exit molar fraction) for the decreasing heat flux profile was almost 25% higher compared to the increasing ramp function and 11% higher compared to the uniform heat flux profile for the net heat input of 533.4 W.

Inlet Flow Rate For the baseline case studied (case C7) as well as in the experiments, the inlet flow rate of the methane-steam mixture was 0.183 g/min and the corresponding mean inlet velocity is 5.06 m/s. This; however, resulted in partial conversion of the methane to hydrogen. The molar conversion of a reactant flowing at a fixed velocity in a heterogeneous chemical reactor of fixed length is dictated by diffusion ($\tau_{\mathrm{d,i}} = (\mathrm{H}/2)^2 / \mathscr{D}_{im}$) and reaction ($\tau_{\mathrm{kin}} = 1/k$) time scales, the ratio of which is embodied in the Damkohler number ($\mathrm{D}a = \tau_{\mathrm{d,i}}/\tau_{\mathrm{kin}}$) [22]. Here H is the channel height; $\mathscr{D}_{im}$ is the diffusion coefficient of species i in mixture m, and k is the reaction rate constant. By measuring the product concentrations, an estimate of the conversion of the reactants to products can be obtained. This conversion is affected by diffusion as well as reaction rates. In addition, the residence time of reactants inside the microchannel is critical and is given by $\tau_{\mathrm{res}} = L/\overline{u}$, where L is the length of the microchannel and $\overline{u}$ is the mean inlet velocity. For the baseline case (C7), the residence time is 0.0263 s whereas the diffusion time scale is 3.93 s. This resulted in methane conversion of only 26.9% based on the inlet and exit molar fractions for the highest heat input.

A series of simulations were performed varying the inlet flow rates till complete conversion of methane to hydrogen was obtained, keeping all other parameters the same. The inlet mean flow velocity for complete conversion was found to be 0.721 m/s corresponding to a flow rate of 0.026 g/min. The corresponding residence time is 0.185 s. With increased residence times, it was observed that the reaction rates steadily increased from the inlet section till the outlet section, resulting in complete conversion. This indicates that for complete conversion, a longer channel (almost five times) would be necessary at the same baseline flow rate used in experiments.

Receiver Shape Optimization

The hydrogen produced by a solar receiver will depend upon the shape of the receiver, the radiative heat transfer occurring within the receiver that results in a heat flux profile along the receiver walls, and the reactions occurring within the microchannels. Ideally, shape optimization of the receiver would entail specifying an initial receiver shape, with Monte-Carlo based radiative heat transfer and ray tracing employed to determine a heat flux profile along the length of the receiver. This heat flux profile would then be employed in a 1-D steady reduced-reaction model to determine the steady state hydrogen output for the receiver shape. In absence of the fully coupled receiver shape-reactor modeling approach to predict hydrogen output, receiver shape optimization is limited in this work to matching a desired heat-flux profile along the length of the receiver. To illustrate the methodology and present approach, a linear heat flux variation along the length of the receiver was used. As shown previously, a decreasing ramp function for the heat flux profile along the microchannel provides the most hydrogen output. However, in the present example, an increasing linear function is used for illustration. As such, the optimization problem examined in this paper reduces to identifying a receiver shape that explicitly matches a prescribed linearly varying heat flux profile along the length of the receiver wall.

In this work, the shape of the solar receiver is assumed symmetric about an axis of revolution, such that the receiver can be designed in two dimensions (r,z). The rear of the receiver is assumed to consist of a flat bottom of radius r_0, located on the r-axis, and the receiver extends for a height h along the z-axis. As stated, the optimization search space contains the set of all possible receiver shapes. To reformulate the maximization problem in a finite, lower-dimensional form that can be numerically solved by sequential quadratic programming (SQP) algorithms, the receiver shape is instead represented by a set of coordinates (r_i,z_i). Chebyshev polynomials are utilized to fit a receiver shape through these points, where r_i represent the radial position of the Chebyshev interpolation points. In this manner, the optimization problem is therefore transformed into one in which the optimization routine must determine the coordinates r_i at each grid point such that a quadratic cost function $J = \mathrm{z}^T\mathbf{Q}\mathrm{z}$ is minimized. The minimization of the cost function is performed subject to design constraints on the radial locations of the interpolation points. In the cost function J, the vector z represents the difference between the heat flux produced by the receiver shape and the desired heat flux profile at prescribed locations along the receiver length and $\mathbf{Q}$ represents a weighting matrix.

Although finite in number, the coordinates (r_i, z_i) produce a continuous receiver shape via the Chebyshev polynomial representation. The resulting constrained, finite dimensional, nonlinear optimization problem is solved in MATLAB using SNOPT, a particularly robust implementation of a SQP algorithm. Provided with an initial guess of the receiver shape, as specified by the radial locations of the Chebyshev interpolation points, a MATLAB function discretizes the receiver shape via piecewise linear polynomials for use in MONT2D, a freely available Monte-Carlo based radiative heat transfer and ray tracing program. These studies use seven Chebyshev points to create the interpolated polynomial which is discretized into 20 surfaces for MONT2D.

MONT2D interprets the radial position of the last Chebyshev point as the radius of the aperture through which solar energy enters the receiver. MONT2D requires a surface to be specified at the aperture so that all of the surfaces form an enclosure. At the aperture surface, MONT2D emits and tracks photons, through possible reflections, until absorption. The aperture is assumed to be a diffuse emitter and a blackbody absorber

as all the photons that hit the aperture surface would be lost to the surroundings. The receiver walls are assumed to be a stainless steel that is a perfectly diffuse reflector and absorbs 50% of incoming photons independent of incident angle. Additionally, all surface properties are assumed to be independent of radiation wavelength. The exchange fraction is defined by $F_i = N_i/N_{\text{total}}$, where F_i is the exchange fraction between the aperture surface and surface i, N_i is the total number of photons absorbed by surface i, and N_{total} is the total number of emitted photons from the aperture surface. The MATLAB code reads the output file from MONT2D and proceeds to calculate a heat flux profile. The total heat flux is specified for the aperture and thus the total radiative energy entering the enclosure is known. The incident radiation for a given surface is given by $q_i = q_{\text{aperture}} * A_{\text{aperture}} * F_i/A_i$, where q_i is the energy flux absorbed by surface i, q_{aperture} is the energy flux entering the aperture, A_{aperture} is the axisymmetric area of the aperture, F_i is the exchange fraction between the aperture surface and surface i, and A_i is the axisymmetric area of surface i. The q_i values form a discrete heat flux profile along the length of receiver wall accounting for the length changes of the receiver based on the wall curvature. This profile is compared to the target linear profile for each surface and the error vector, z, is calculated as the absolute value of the difference between the calculated heat flux and the target heat flux normalized by the number of surfaces. For these studies the weighting matrix $\mathbf{Q}$ was the identity matrix.

SNOPT was subsequently responsible for determining new values for the radial locations of the Chebyshev interpolation points and this process was repeated until the cost function, subject to the bounds on the values for the interpolation points, was minimized. The efficacy of this strategy is illustrated through its ability to identify a receiver shape that produced a heat flux profile that varied linearly along the length of the receiver, as illustrated in figure 3a. The optimized shape is shown in figure 3b. The heat flux profile is independent of length scale and scales linearly with the aperture heat flux for a constant aspect ratio.

These results show that it is possible to closely match a linear heat flux profile with a combination of SNOPT and MONT2D. The average and maximum error between the calculated and target heat flux profiles are 1.2% and 11.9% respectively. While this final error is small, there are two factors that reduce the robustness of this method. Appropriate values require an iterative approach by the user. Additionally, the precision of Monte-Carlo results somewhat interferes with the SNOPT optimization routine. This routine works best with smooth or nearly-smooth functions. By their stochastic nature, Monte Carlo methods do not produce smooth results. Using the same inputs, executing MONT2D twice will produce slightly different answers. This difference reduces robustness especially when SNOPT estimates derivatives of the objective function, J, using finite difference approximations. To mitigate this effect, the number of photons emitted by MONT2D was increased to a value on the order of 10^8. This significantly increased the computational expense of evaluating J, but was necessary for SNOPT to find an acceptable solution.

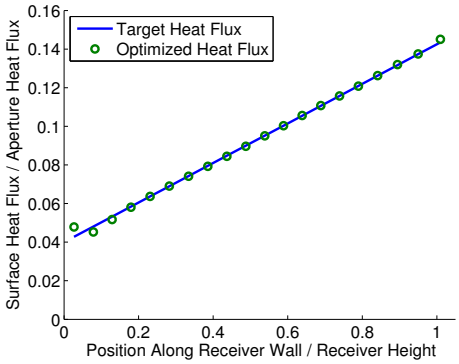

(a)

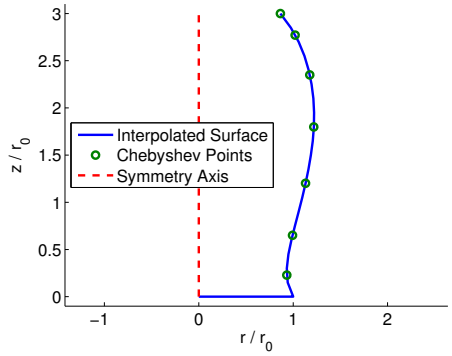

(b)

FIGURE 3: Receiver shape optimization for a specified heat flux profile: (a) plot showing the matching of the optimum calculated heat flux profile to the target profile. Heat flux values are normalized by the aperture heat flux and the length is normalized by the receiver height; (b) shape that returned the minimum error.

SUMMARY & CONCLUSION

Numerical experiments investigating effectiveness of a microchannel reactor geometry on methane-steam reforming are performed using a simple steady-state one-dimensional model with multicomponent heterogeneous reactions. Methane-steam reforming is modeled by three reduced-order reactions occurring on the reactor walls, two of which are endothermic reactions and an exothermic water-gas shift reaction.

First the numerical model was applied to predict hydrogen production in a microchannel setup based on the experimental setup of Eilers [1] and validated against the DNS calculations performed by co-workers [11] to show good predictive capability. Parametric studies were then performed by varying the net heat input, heat flux profile along the microchannel, and the in-

let flow rate to study their effect on the methane conversion.For a given flow rate and heat input, a decreasing ramp function for the heat flux along the microchannel yielded increased hydrogen production. By controlling the inlet flow rates that alter the residence time compared to the reaction time scales, complete conversion of CH_4 to H_2 was feasible.

Finally, a shape-constrained optimization procedure using the SNOPT algorithm coupled with the radiative heat transfer module MONT2D [12] was developed to design the receiver shape that provides a desired heat flux profile along the microchannel length. This optimization process can be used to design receiver shapes for optimal hydrogen production.

ACKNOWLEDGMENT

This work was funded partly by the Oregon Best Solar energy initiative and partly by US Army through the Oregon Nano and Microtechnology Institute (ONAMI). We also thank Prof. Murty Kanury of OSU for several useful discussions related to combustion and chemical kinetics modeling.

REFERENCES

[1] Eilers, B., 2010. "Microchannel steam-methane reforming under constant and variable surface temperature distributions". *M.S. Thesis, Oregon State University*.

[2] Eiler, B., Narayanan, V., Apte, S., and Schmitt, J., 2011. "Steam-methabe reforming in a microchannel under constant and variable surface temperature profiles". In AJTEC2011-44390, Proceedings of the ASME/JSME 2011 8th Thermal Engineering Joint Conference, Honolulu, Hawaii, USA.

[3] Tamme, R., Buck, R., Epstein, M., Fisher, U., and Sugarmen, C., 2001. "Solar upgrading of fuels for generation of electricity". *Journal of Solar Energy Engineering,* ***123***, p. 160.

[4] Möller, S., Kaucic, D., and Sattler, C., 2006. "Hydrogen production by solar reforming of natural gas: a comparison study of two possible process configurations". *Journal of Solar Energy Engineering,* ***128***, p. 16.

[5] Kodama, T., Moriyama, T., Shimoyama, T., Gokon, N., Andou, H., and Satou, N., 2006. "Ru/ Ni–Mg–O catalyzed SiC-foam absorber for solar reforming receiver-reactor". *Journal of Solar Energy Engineering,* ***128***, p. 318.

[6] Wegeng, R., TeGrotenhuis, W., and Mankins, J., 2007. "Solar thermochemical production of fuels". *AIAA, 2007-4709, 5th International Energy Conversion Engineering Conference and Exhibit.*

[7] Wegeng, R., and Mankins, J., 2009. "Space power systems: Producing transportation (and other chemical) fuels as an alternative to electricity generation". *Acta Astronautica,* ***65***(9-10), pp. 1261–1271.

[8] Steinfeld, A., 2005. "Solar thermochemical production of hydrogen—-a review". *Solar Energy,* ***78***(5), pp. 603–615.

[9] Röger, M., Pfander, M., and Buck, R., 2006. "Multiple air-jet window cooling for high-temperature pressurized volumetric receivers: Testing, evaluation, and modeling". *Journal of Solar Energy Engineering,* ***128***(3), pp. 265–274.

[10] Kraupl, S., and Steinfeld, A., 2001. "Pulsed gas feeding for stoichiometric operation of a gas-solid vortex flow solar chemical reactor". *Journal of Solar Energy Engineering,* ***123***, p. 133.

[11] Drost, K., Eiler, B., Peterson, D., Apte, S., Narayanan, V., and Schmitt, J., 2011. "Detailed numerical modeling of a microchannel reactor for methane-steam reforming". In AJTEC2011-44664, Proceedings of the ASME/JSME 2011 8th Thermal Engineering Joint Conference, Honolulu, Hawaii, USA.

[12] Maltby, J., Zeeb, C., Dolaghan, J., and Burns, P., 1994. "Users manual for MONT2D-version 2.6 and MONT3D-version 2.3". *Department of Mechanical Engineering, Colorado State University, Fort Collins, CO*.

[13] Shu, J., Grandjean, B., and Kaliaguine, S., 1994. "Methane Steam Reforming in Asymmetric Pd-Ag and Pd-Ag/Porous SS Membrane Reactors". *Applied Catalysis A: General,* ***119***(2), pp. 305–325.

[14] Deutschmann, O., and Schmidt, L., 1998. "Modeling the partial oxidation of methane in a short-contact-time reactor". *AIChE Journal,* ***44***(11), pp. 2465–2477.

[15] Kuznetsov, V., and Kozlov, S., 2008. "Modeling of methane steam reforming in a microchannel with a heat flow distributed in length". *Journal of Engineering Thermophysics,* ***17***(1), pp. 53–59.

[16] Wang, Y., Yoshiba, F., Kawase, M., and Watanabe, T., 2009. "Performance and effective kinetic models of methane steam reforming over Ni/YSZ anode of planar SOFC". *International Journal of Hydrogen Energy,* ***34***(9), pp. 3885–3893.

[17] Xu, J., and Froment, G., 1989. "Methane steam reforming, methanation and water-gas shift: I. Intrinsic kinetics". *AIChE Journal,* ***35***(1), pp. 88–96.

[18] Hou, K., and Hughes, R., 2001. "The kinetics of methane steam reforming over a Ni/α-Al2O catalyst". *Chemical Engineering Journal,* ***82***(1-3), pp. 311–328.

[19] Kenneth, K., 2005. "Principles of combustion". *John Wiley's sons, Ine, Hoboken, New Jersey*.

[20] Turns, S., 1995. "An introduction to combustion: Concepts and applications(Book)". *New York: McGraw-Hill, Inc, 1995.*

[21] Kanury, A., 1984. "Introduction to combustion phenomena". *Gordon and Breach Science Publishers, New York,* ***Fourth printing***.